

Observational Constraints to Ricci Dark Energy Model by Using: SN, BAO, OHD, fgas Data Sets

Lixin Xu* and Yuting Wang†

*School of Physics and Optoelectronic Technology,
Dalian University of Technology, Dalian, Liaoning 116024, P. R. China*

In this paper, we perform a global constraint on the Ricci dark energy model with both the flat case and the non-flat case, using the Markov Chain Monte Carlo (MCMC) method and the combined observational data from the cluster X-ray gas mass fraction, Supernovae of type Ia (397), baryon acoustic oscillations, current Cosmic Microwave Background, and the observational Hubble function. In the flat model, we obtain the best fit values of the parameters in $1\sigma, 2\sigma$ regions: $\Omega_{m0} = 0.2927^{+0.0420+0.0542}_{-0.0323-0.0388}$, $\alpha = 0.3823^{+0.0331+0.0415}_{-0.0418-0.0541}$, $Age/Gyr = 13.48^{+0.13+0.17}_{-0.16-0.21}$, $H_0 = 69.09^{+2.56+3.09}_{-2.37-3.39}$. In the non-flat model, the best fit parameters are found in $1\sigma, 2\sigma$ regions: $\Omega_{m0} = 0.3003^{+0.0367+0.0429}_{-0.0371-0.0423}$, $\alpha = 0.3845^{+0.0386+0.0521}_{-0.0474-0.0523}$, $\Omega_k = 0.0240^{+0.0109+0.0133}_{-0.0130-0.0153}$, $Age/Gyr = 12.54^{+0.51+0.65}_{-0.37-0.49}$, $H_0 = 72.89^{+3.31+3.88}_{-3.05-3.72}$. Compared to the constraint results in the Λ CDM model by using the same datasets, it is shown that the current combined datasets prefer the Λ CDM model to the Ricci dark energy model.

PACS numbers: 98.80.-k, 98.80.Es

Keywords: dark energy, constraints

I. INTRODUCTION

The observation of the Supernovae of type Ia (SN Ia) [1, 2] provides the evidence that the universe is undergoing accelerated expansion. Jointing current Cosmic Microwave Background (CMB) anisotropy measurement from Wilkinson Microwave Anisotropy Probe (WMAP) [3, 4] and the data of the Large Scale Structure (LSS) from SDSS [5, 6], one concludes that there exists an exotic energy component with negative pressure, dubbed dark energy, whose density accounts for two-thirds of the total energy density in the universe at present. The simplest but most natural candidate of dark energy is the cosmological constant Λ , with the constant equation of state $w_\Lambda = -1$. In fact, the observational data is mostly consistent with the predictions of the Λ CDM model [7–9]. However, it suffers the so-called fine tuning and cosmic coincidence problems. To avoid these problems, dynamic dark energy models are considered as an alternative scenario, such as quintessence [10–15], phantom [16], quintom [17] and holographic dark energy [18, 19] etc.

Although more and more dark energy models have been presented, the nature of dark energy is still a conundrum. Under such circumstances, the models which are built according to some fundamental principle are more charming, such as holographic dark energy model and agegraphic dark energy model [20, 21]. The former one is on the basis of holographic principle, and the latter one is derived from taking the combination between the uncertainty relation in quantum mechanics and general relativity into account. In this paper, we focus on the holographic dark energy model, which is considered as a dynamic vacuum energy and constructed by considering the holographic principle and some features of quantum gravity theory. According to the holographic principle, the number of degrees of freedom in a bounded system should be finite and has relations with the area of its boundary. By applying the principle to cosmology, one can obtain the upper bound of the entropy contained in the universe. For a system with size L and UV cut-off Λ without decaying into a black hole, it is required that the total energy in a region of size L should not exceed the mass of a black hole of the same size, thus $L^3 \rho_\Lambda \leq LM_{pl}^2$. The largest L allowed is the one saturating this inequality, thus

$$\rho_\Lambda = \frac{3c^2 M_{pl}^2}{L^2}, \quad (1)$$

where c is a numerical constant and M_{pl} is the reduced Planck Mass $M_{pl} \equiv 1/\sqrt{8\pi G}$. It just means a duality between UV cut-off and IR cut-off. The UV cut-off is related to the vacuum energy, and IR cut-off is related to the large scale of the universe, for example Hubble horizon, event horizon or particle horizon as discussed by [18, 19].

*Electronic address: lxxu@dlut.edu.cn

†Electronic address: wangyuting0719@163.com

In the paper [19], the author took the future event horizon

$$R_{eh}(a) = a \int_t^\infty \frac{dt'}{a(t')} = a \int_a^\infty \frac{da'}{Ha'^2} \quad (2)$$

as the IR cut-off L . Although this model is confronted with the causality problem, as pointed out in [19], it can reveal the dynamic nature of the vacuum energy and provide a solution to the fine tuning and cosmic coincidence problem. When $c \geq 1$, $c = 1$ and $c \leq 1$, the holographic dark energy behaves like quintessence, cosmological constant and phantom respectively. Therefore, in this model, the value of parameter c plays an important role in determining the property of holographic dark energy. Then, a model with holographic dark energy proportional to the Ricci scalar was proposed by Gao, et. al. in [22], called the Ricci dark energy (RDE). In that paper [22], it has shown that this model can avoid the causality problem and naturally solve the coincidence problem of dark energy after Ricci scalar is regarded as the IR cut-off L^{-2} :

$$L^{-2} = R = -6(\dot{H} + 2H^2 + \frac{k}{a^2}). \quad (3)$$

An fascinating aspect in the study of dark energy is that the cosmological parameters in a given model can be constrained by the increasing observational data. It is found that the best way to constrain is using the combination of a thorough observation. Now we give a brief review of the previous works on the combined observational constraints of the Ricci dark energy model. In Ref. [23], we constrained the parameters Ω_{m0} and α using 192 SN Ia data [8] from the ESSENCE [24] and Gold sets [25–27], the CMB shift parameter R from three-year WMAP data [28], and the BAO parameter A from SDSS [29], obtaining the best-fittings: $\Omega_{m0} = 0.34 \pm 0.04$ and $\alpha = 0.38 \pm 0.03$. Subsequently, the authors in Ref. [30, 31] utilized the latest 307 Union SNIa data from the Supernova Cosmology Project (SCP), the updated shift parameter R from the five-year WMAP data [32], and the independent form of the SDSS BAO parameter A [29] to constrain the parameters Ω_{m0} and α , whose best-fit values are given by $\Omega_{m0} = 0.318_{-0.024}^{+0.026}$ and $\alpha = 0.359_{-0.025}^{+0.024}$ in [30]. In Ref. [33], the SDSS BAO parameter A is replaced by the measurement of $D_V(0.35)/D_V(0.2)$ from SDSS [34] to investigate the generalized Ricci dark energy model. Then Li, et. al in [35] used the extended 397 SNIa data from the Union+CFA3 sample [36], only the values of $[r_s(z_d)/D_V(0.2), r_s(z_d)/D_V(0.35)]$ in the measurement of BAO [37] and the Maximum likelihood values of $[l_A(z_*), R(z_*), z_*]$ and their inverse covariance matrix in the measurement of CMB [32], getting the best constraint results: $\Omega_{m0} = 0.304, \alpha = 0.363$.

In this paper, we will revisit the RDE model and make a thorough investigation on this model with a completely consistent analysis of the combined observations. Comparing with the previous works, we use the more complete combinations of the observational datasets from the X-ray gas mass fraction in clusters of galaxies (CBF) [38], 397 SN Ia [36] data, the BAO measurement on the values of $[r_s(z_d)/D_V(0.2), r_s(z_d)/D_V(0.35)]$ and their inverse covariance matrix in [37], the CMB observation [32] on the Maximum likelihood values of $[l_A(z_*), R(z_*), z_*]$ and their inverse covariance matrix and the observational Hubble data at fifteen different redshifts, including the three more observational data $H(z = 0.24) = 79.69 \pm 2.32$, $H(z = 0.34) = 83.8 \pm 2.96$, and $H(z = 0.43) = 86.45 \pm 3.27$ in [39] and the observational data [40, 41]. We carry out the global fitting on the RDE model using the Markov Chain Monte Carlo (MCMC) method. In addition, in this paper we do not only perform the constraint on the parameters in the flat RDE model, but also in the non-flat RDE model, comparing with the constraint results in the standard concordance model by using the same combined datasets.

The paper is organized as follows. In next section, we briefly review the RDE model. In section III, we describe the method and data. After we perform the cosmic observation constraint, the results on the determination of the cosmological parameters are presented. The last section is the conclusion.

II. REVIEW THE RICCI DARK ENERGY MODEL

In this section, we give a brief review on the general formula in the RDE model. With a Friedmann-Robertson-Walker (FRW) metric

$$ds^2 = -dt^2 + a^2(t) \left[\frac{dr^2}{1 - kr^2} + r^2(d\theta^2 + \sin^2\theta d\phi^2) \right], \quad (4)$$

the Einstein field equation can be written as

$$H^2 = \frac{1}{3M_{pl}^2}(\rho_m + \rho_R) - \frac{k}{a^2}, \quad (5)$$

model parameters	flat RDE	flat Λ CDM	not-flat RDE	non-flat Λ CDM
Ω_{m0}	$0.2927^{+0.0420+0.0542}_{-0.0323-0.0388}$	$0.2778^{+0.0268+0.0396}_{-0.0323-0.0379}$	$0.3003^{+0.0367+0.0429}_{-0.0371-0.0423}$	$0.2730^{+0.0352+0.0424}_{-0.0303-0.0330}$
α	$0.3823^{+0.0331+0.0415}_{-0.0418-0.0541}$	-	$0.3845^{+0.0386+0.0521}_{-0.0474-0.0523}$	-
Ω_k	-	-	$0.0240^{+0.0109+0.0133}_{-0.0130-0.0153}$	$-0.0010^{+0.0106+0.0135}_{-0.0105-0.0139}$
Age/Gyr	$13.48^{+0.13+0.17}_{-0.16-0.21}$	$13.71^{+0.11+0.13}_{-0.13-0.16}$	$12.54^{+0.51+0.65}_{-0.37-0.49}$	$13.75^{+0.51+0.65}_{-0.48-0.59}$
H_0	$69.09^{+2.56+3.09}_{-2.37-3.39}$	$70.23^{+2.56+3.19}_{-1.91-2.70}$	$72.89^{+3.31+3.88}_{-3.05-3.72}$	$70.38^{+2.69+3.18}_{-2.70-3.57}$
χ^2_{min}	562.543	521.669	539.763	521.557

TABLE I: The data fitting results of the parameters with 1σ , 2σ regions in RDE model and the Λ CDM model, where the combined observational data from CBF, SN, BAO and CMB and OHD are used.

where the parameter k denotes the curvature of space $k = 1, 0, -1$ for closed, flat and open geometries, respectively, H is the Hubble function, and ρ is the energy density of a general piece of matter, and their subscripts m and R respectively correspond to matter component, including the cold dark matter ρ_{cdm} and baryon matter ρ_b , and RDE.

As suggested by Gao et. al., the energy density of RDE is proportional to the Ricci scalar, thus whose energy density is given as

$$\rho_R = 3\alpha M_{pl}^2 (\dot{H} + 2H^2 + \frac{k}{a^2}) \propto R, \quad (6)$$

where α is the dimensionless parameter in RDE model, which can be determined though cosmic observation constraints. After changing the variable from the cosmic time t to $x = \ln a$, we can rewritten the Friedmann Eq. (5) as

$$H^2 = \frac{1}{3M_{pl}^2} \rho_{m0} e^{-3x} + (\alpha - 1) k e^{-2x} + \alpha \left(\frac{1}{2} \frac{dH^2}{dx} + 2H^2 \right). \quad (7)$$

With the help of the definitions as follows:

$$E = \frac{H}{H_0}, \Omega_{m0} = \frac{\rho_{m0}}{3M_{pl}^2 H_0^2}, \Omega_k = -\frac{k}{H_0^2}, \quad (8)$$

the Eq. (7) can be ulteriorly rewritten as

$$E^2 = (1 - \alpha) \Omega_k e^{-2x} + \Omega_{m0} e^{-3x} + \alpha \left(\frac{1}{2} \frac{dE^2}{dx} + 2E^2 \right). \quad (9)$$

Solving this first order differential equation about E^2 , we can obtain

$$\begin{aligned} E^2 &= \Omega_k e^{-2x} + \Omega_{m0} e^{-3x} + \frac{\alpha}{2 - \alpha} \Omega_{m0} e^{-3x} + f_0 e^{-(4 - \frac{2}{\alpha})x} \\ &= \Omega_k e^{-2x} + \Omega_{m0} e^{-3x} + \Omega_R(x), \end{aligned} \quad (10)$$

where f_0 is the integral constant and can be derived by the initial condition $E(x=0) = 1$, i.e. $\Omega_k + \Omega_{m0} + \Omega_{R0} = 1$ is used, which is $f_0 = 1 - \Omega_k - \frac{2}{2-\alpha} \Omega_{m0}$, and Ω_R is the definition of the dimensionless RDE density, with the expression being

$$\Omega_R(x) = \frac{\alpha}{2 - \alpha} \Omega_{m0} e^{-3x} + \left(1 - \Omega_k - \frac{2}{2 - \alpha} \Omega_{m0} \right) e^{-(4 - \frac{2}{\alpha})x}. \quad (11)$$

III. METHOD AND RESULTS

In our analysis, we perform a global fitting on determining the cosmological parameters using the Markov Chain Monte Carlo (MCMC) method. The MCMC method is based on the publicly available **CosmoMC** package [42] and the **modified CosmoMC** package [38, 43, 44], including the X-ray cluster gas mass fraction. For our models we has modified these packages to add the new parameter α with a prior $\alpha \in [0.1, 0.8]$. Besides the parameter α , the following basic cosmological parameters ($\Omega_b h^2$, $\Omega_c h^2$, Ω_k) are also varying with top-hat priors: the physical baryon

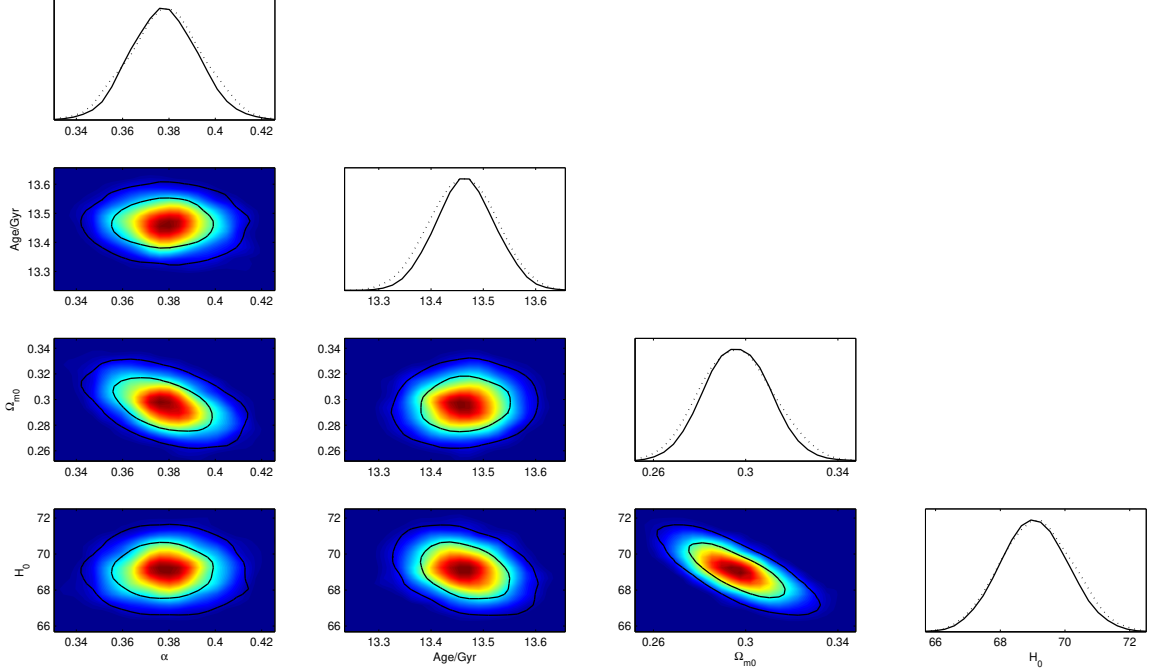


FIG. 1: 1-D constraints on individual parameters (α , Age/Gyr , Ω_{m0} , H_0) and 2-D contours on these parameters with 1σ , 2σ errors between each other using the combination of the observational data from CBF, SN, BAO, CMB and OHD in the flat RDE model. Dotted lines in the 1-D plots show the mean likelihood of the samples and the solid lines are marginalized probabilities for the parameters in the flat RDE model [42].

density $\Omega_b h^2 \in [0.005, 0.1]$, the physical dark matter energy density $\Omega_c h^2 \in [0.01, 0.99]$, and the density of space curvature $\Omega_k \in [-0.1, 0.1]$. The cosmological parameter Ω_{m0} can be derived from the basic parameters above. We use a top-hat prior of the cosmic age i.e. $10Gyr < t_0 < 20Gyr$ and impose a weak Gaussian prior on the physical baryon density $\Omega_b h^2 = 0.022 \pm 0.002$ from Big Bang nucleosynthesis [45]. Also, in the data fitting process the seven parameters ($K, \eta, \gamma, b_0, \alpha_b, s_0, \alpha_s$) included in the X-ray gas mass fraction f_{gas} are treated as free parameters. As a byproduct the best fitting values of these parameters are obtained. And, these values can also be taken accounted as a check of data fitting.

In our calculations, we have taken the total likelihood function $L \propto e^{-\chi^2/2}$ to be the products of the separate likelihoods of CBF, SN, BAO, CMB and OHD. Then we get χ^2 is

$$\chi^2 = \chi_{CBF}^2 + \chi_{SN}^2 + \chi_{BAO}^2 + \chi_{CMB}^2 + \chi_{OHD}^2, \quad (12)$$

where the separate likelihoods of CBF, SN, BAO, CMB and OHD and the current observational datasets used in this paper are shown in the Appendix A.

The results on the best values of the cosmological parameters with 1σ , 2σ errors in the RDE model and the Λ CDM model are listed in Table I. In the Fig. 1, we show one dimensional probability distribution of each parameter and two dimensional plots for parameters between each other in the flat RDE model. The corresponding plots in the non-flat RDE model are presented in Fig. 2. From Figs. 1 and 2, it is seen that the cosmological parameters in the two cases of RDE model are well determined in 1σ and 2σ regions. Comparing the flat RDE model with the non-flat RDE model, we can find the difference of χ_{min}^2 is obvious. The non-flat RDE model with a smaller $\chi_{min}^2 = 539.763$ is favored over the flat case with $\chi_{min}^2 = 562.543$. However, compared to the Λ CDM model, it is found the Λ CDM models with smaller values $\chi_{min}^2 = 521.669$ (flat case) and $\chi_{min}^2 = 521.557$ (non-flat case) are better fit to the current combined data than the RDE model. What is more, we obtain the best-fit values of the parameters in f_{gas} : $K = 0.9665, \eta = 0.2058, \gamma = 1.0866, b_0 = 0.7073, \alpha_b = -0.0540, s_0 = 0.1654, \alpha_s = 0.1591$ in the flat case and $K = 0.9871, \eta = 0.2114, \gamma = 1.0507, b_0 = 0.7749, \alpha_b = -0.0950, s_0 = 0.1741, \alpha_s = 0.0194$ in the non-flat case.

From Fig. 3, we can see the constraints on the parameters (α , Ω_{m0}) in the flat RDE model by using the independent dataset from CBF (black solid), SN (red), BAO (blue), CMB (magenta) and OHD (green) and the combined datasets

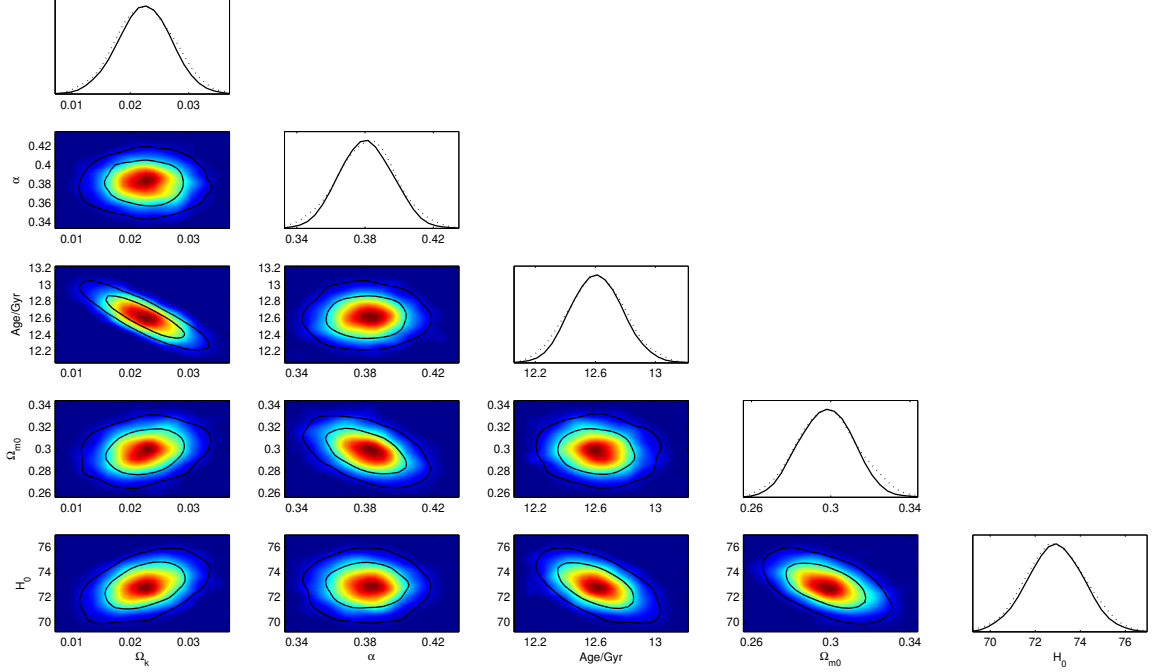


FIG. 2: 1-D constraints on individual parameters ($\Omega_k, \alpha, Age/Gyr, \Omega_{m0}, H_0$) and 2-D contours on these parameters with $1\sigma, 2\sigma$ errors between each other using the combination of the observational data from CBF, SN, BAO, CMB and OHD in the non-flat RDE model. Dotted lines in the 1-D plots show the mean likelihood of the samples and the solid lines are marginalized probabilities for the parameters in the non-flat RDE model [42].

(black dotted). It is found all the constraint results from the independent dataset are consistent. It is obvious that the space of the parameters (α, Ω_{m0}) has been reduced by using the three combined datasets from SN, BAO and CMB (cyan). It is indicated that the tight constraint has been obtained by the three combined datasets. Combined with the additional datasets from CBF and OHD, it is seen that the best fit values of the parameters are changed. For the parameters (α, Ω_{m0}), the inclusion of the datasets from CBF and OHD changes their best fit values from (0.3630, 0.3192) to (0.3823, 0.2927). In addition, as shown in Fig. 3, though the degeneracy with the additional datasets from CBF and OHD is not obviously improved, the curves of the 2-D contour plot from the five combined datasets become smoother than that from the three combined datasets.

Next, we investigate the models according to the objective Information Criterion (IC) including the Akaike Information Criterion (AIC) and Bayesian Information Criterion (BIC). Here, we give a brief introduction, for the details please see in Ref. [46–50]. The AIC was based on the Kullback-Leibler information entropy and derived by H. Akaike. It takes the form

$$AIC = -2 \ln \mathcal{L}(\hat{\theta}|data)_{max} + 2K, \quad (13)$$

where, \mathcal{L}_{max} is the highest likelihood in the model with the best fit parameters $\hat{\theta}$, K is the number of parameters in the model. The first term of Eq. (13) measures the goodness of model fit, and the second one interprets model complexity. The BIC is similar as AIC, but the second term is different. It was derived by G. Schwarz and is given by the form

$$BIC = -2 \ln \mathcal{L}(\hat{\theta}|data)_{max} + K \ln n, \quad (14)$$

where, n in the different term is the number of data points in the datasets. In the above two cases, the term $-2 \ln \mathcal{L}(\hat{\theta}|data)_{max}$ is often called χ^2_{min} , though it is also generalized to non-Gaussian distributions.

Now, the problem is how to evaluate which model is the better one. It is the issue of strength of evidence. We take AIC case as an example. And, BIC is the same as that. Comparing the AIC values of several models, the minimum one is considered as the best value and denoted by $AIC_{min} = \min\{AIC_i, i = 1 \dots N\}$, where $i = 1 \dots N$ is a set of

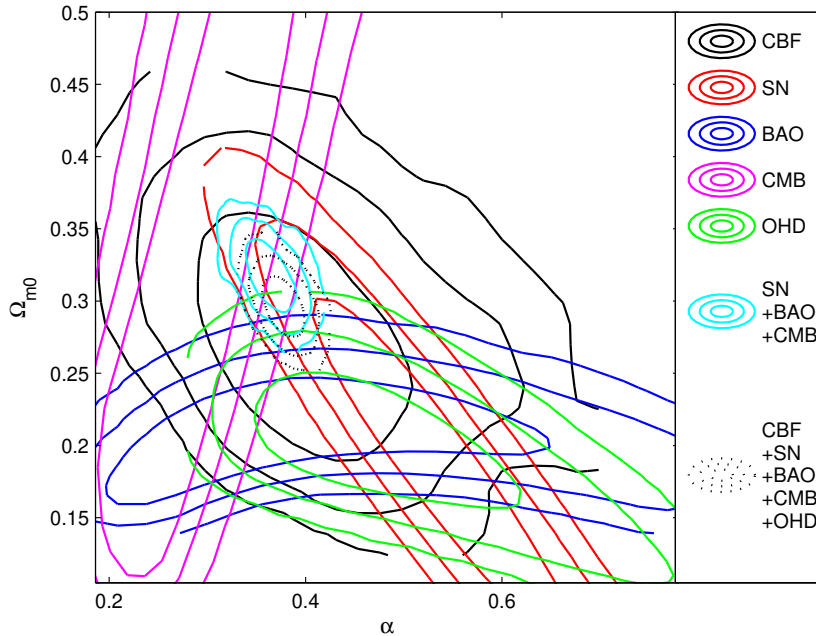


FIG. 3: The 2-D contours on the parameters (α, Ω_{m0}) with 1σ , 2σ and 3σ confidence in the flat RDE model for CBF only (black solid line), SN only (red line), BAO only (blue line), CMB only (magenta line), OHD only (green line). The joint constraint from SN, BAO and CMB is shown in cyan line and the fully combined constraint from CBF, SN, BAO, CMB, and OHD is shown in black dotted line.

alternative candidate models. The difference of AIC for other alternative model i with respect to the basic model is expressed as $\Delta AIC_i = AIC_i - AIC_{min}$. The rules of judgement of AIC model selection are that when ΔAIC_i is in the range $0 - 2$, it means the model i has almost the same supports from the data as the best one; for the range $2 - 4$, this support is considerably less and with $\Delta AIC_i > 10$ model i is practically irrelevant [46]. For BIC, the rules read that a ΔBIC of more than 2 (or 6) relative to the best one is considered "unsupported" (or "strongly unsupported") from observational data [47].

Model	Parameters	χ^2_{min}	AIC	ΔAIC	BIC	ΔBIC
flat Λ CDM	9	521.669	539.669	0	576.83	0
non-flat Λ CDM	10	521.557	541.557	1.888	582.848	6.017
flat RDE	10	562.543	582.543	42.874	623.834	47.003
non-flat RDE	11	539.763	561.763	22.094	607.183	30.352

TABLE II: The results of χ^2_{min} , AIC and BIC in the Λ CDM model and RDE model and the differences of AIC and BIC with respect to the flat Λ CDM model are listed.

The values of AIC and BIC in the Λ CDM model and RDE model and the differences of AIC and BIC with respect to the flat Λ CDM model are listed in Table II. In the table, it reads the flat Λ CDM model are favored by both AIC and BIC. According to the rules of judgement of AIC model selection above, it is seen that the non-flat Λ CDM model is supported considerably and the RDE models are disfavored. Since BIC imposes a stricter penalty against introducing extra parameters than AIC, as shown from Eq. (14), all the models except the flat Λ CDM model are disfavored by BIC.

IV. CONCLUSION

In summary, in this paper we have performed a global fitting on the cosmological parameters in both the flat RDE model and the non-flat RDE model by using a completely consistent analysis of the X-ray gas mass fraction

observation, type Ia supernovae data from the combination of CfA3 samples and the Union set, baryon acoustic oscillations data from SDSS, the measurement data on current Cosmic Microwave Background from the five-year WMAP observations and the observational Hubble data. The constraint on the parameters in the Λ CDM model are performed by using the same combined datasets. The constraint results are shown in Table I for the flat RDE model $\chi^2_{min} = 562.543$, for the non-flat RDE model $\chi^2_{min} = 539.763$, for the flat Λ CDM model $\chi^2_{min} = 521.669$, and for the non-flat Λ CDM model $\chi^2_{min} = 521.557$. From Fig. 3, it is shown that the best fit values of the parameters (α, Ω_{m0}) are changed by the additional datasets from CBF and OHD, though the additional data have a minor effect on the confidences of the parameters. It is indicated that more accurate data is anticipated to provide the more stringent constraint on the parameters in RDE model. Comparing the RDE model with the Λ CDM model, we can find that the current combined datasets do favor the Λ CDM model over the RDE model. According to AIC and BIC, we find that the flat Λ CDM model is much supported by the current data. The RDE model is disfavored by AIC and BIC.

Acknowledgments

The data fitting is based on the publicly available **CosmoMC** package a Markov Chain Monte Carlo (MCMC) code. This work is supported by the National Natural Science Foundation of China (Grant No 10703001), and Specialized Research Fund for the Doctoral Program of Higher Education (Grant No 20070141034).

Appendix A: Cosmological Constraints Methods

1. The X-ray gas mass fraction constraints

According to the X-ray cluster gas mass fraction observation, the baryon mass fraction in clusters of galaxies (CBF) can be utilized to constrain cosmological parameters. The X-ray gas mass fraction, f_{gas} , is defined as the ratio of the X-ray gas mass to the total mass of a cluster, which is approximately independent on the redshift for the hot ($kT \gtrsim 5keV$), dynamically relaxed clusters at the radii larger than the innermost core r_{2500} . The X-ray gas mass fraction, f_{gas} , can be derived from the observed X-ray surface brightness profile and the deprojected temperature profile of X-ray gas under the assumptions of spherical symmetry and hydrostatic equilibrium. Basing on these assumptions above, Allen et al. [38] selected 42 hot ($kT \gtrsim 5keV$), X-ray luminous, dynamically relaxed clusters for f_{gas} measurements. The stringent restriction to the selected sample can not only reduce maximally the effect of the systematic scatter in f_{gas} data, but also ensure that the f_{gas} data is independent on temperature. In the framework of the Λ CDM reference cosmology, the X-ray gas mass fraction is presented as [38]

$$f_{gas}^{\Lambda CDM}(z) = \frac{KA\gamma b(z)}{1+s(z)} \left(\frac{\Omega_b}{\Omega_m} \right) \left[\frac{d_A^{\Lambda CDM}(z)}{d_A(z)} \right]^{1.5}, \quad (A1)$$

where A is the angular correction factor, which is caused by the change in angle for the current test model θ_{2500} in comparison with that of the reference cosmology $\theta_{2500}^{\Lambda CDM}$:

$$A = \left(\frac{\theta_{2500}^{\Lambda CDM}}{\theta_{2500}} \right)^\eta \approx \left(\frac{H(z)d_A(z)}{[H(z)d_A(z)]^{\Lambda CDM}} \right)^\eta, \quad (A2)$$

here, the index η is the slope of the $f_{gas}(r/r_{2500})$ data within the radius r_{2500} , with the best-fit average value $\eta = 0.214 \pm 0.022$ [38]. And the angular diameter distance is given by

$$d_A(z) = \frac{c}{(1+z)\sqrt{|\Omega_k|}} \text{sinn}[\sqrt{|\Omega_k|} \int_0^z \frac{dz'}{H(z')}], \quad (A3)$$

where $\text{sinn}(\sqrt{|\Omega_k|x})$ respectively denotes $\sin(\sqrt{|\Omega_k|x})$, $\sqrt{|\Omega_k|x}$, $\sinh(\sqrt{|\Omega_k|x})$ for $\Omega_k < 0$, $\Omega_k = 0$ and $\Omega_k > 0$.

In equation (A1), the parameter γ denotes permissible departures from the assumption of hydrostatic equilibrium, due to non-thermal pressure support; the bias factor $b(z) = b_0(1 + \alpha_b z)$ accounts for uncertainties in the cluster depletion factor; $s(z) = s_0(1 + \alpha_s z)$ accounts for uncertainties of the baryonic mass fraction in stars and a Gaussian prior for s_0 is employed, with $s_0 = (0.16 \pm 0.05)h_{70}^{0.5}$ [38]; the factor K is used to describe the combined effects of the residual uncertainties, such as the instrumental calibration and certain X-ray modelling issues, and a Gaussian prior for the 'calibration' factor is considered by $K = 1.0 \pm 0.1$ [38];

Following the method in Ref. [38, 51] and adopting the updated 42 observational f_{gas} data in Ref. [38], the best fit values of the model parameters for the X-ray gas mass fraction analysis are determined by minimizing,

$$\chi_{CBF}^2 = \sum_i^N \frac{[f_{gas}^{\Lambda\text{CDM}}(z_i) - f_{gas}(z_i)]^2}{\sigma_{f_{gas}}^2(z_i)}, \quad (\text{A4})$$

where $\sigma_{f_{gas}}(z_i)$ is the statistical uncertainties (Table 3 of [38]). As pointed out in [38], the acquiescent systematic uncertainties have been considered according to the parameters i.e. $\eta, b(z), s(z)$ and K .

2. Type Ia Supernovae constraints

We use the 397 SN Ia Constitution dataset [36]. The 90 SN Ia from CfA3 sample with low redshifts are added to 307 SN Ia Union sample [52]. The CfA3 sample increases the number of the nearby SN Ia and reduces the statistical uncertainties. In our analysis we use the Constitution datasets used SALT fitter [53] to fit the SN Ia light curves, where the intrinsic uncertainty of 0.138 mag for each CfA3 SNIa, the peculiar velocity uncertainty of 400km/s, and the redshift uncertainty of 0.001 have been considered to realize a more cautious assumption that there is the same Hubble residual uncertainty between the CfA3 SN and the nearby Union SN [36]. Following [54, 55], one can obtain the corresponding constraints by fitting the distance modulus $\mu(z)$ as

$$\mu_{th}(z) = 5 \log_{10}[D_L(z)] + \mu_0. \quad (\text{A5})$$

In this expression $D_L(z)$ is the Hubble-free luminosity distance $H_0 d_L(z)/c = H_0 d_A(z)(1+z)^2/c$, with H_0 the Hubble constant, defined through the re-normalized quantity h as $H_0 = 100h \text{ km s}^{-1} \text{ Mpc}^{-1}$, and $\mu_0 \equiv 42.38 - 5 \log_{10} h$.

Additionally, the observed distance moduli $\mu_{obs}(z_i)$ of SN Ia at z_i is

$$\mu_{obs}(z_i) = m_{obs}(z_i) - M, \quad (\text{A6})$$

where M is their absolute magnitudes.

For the SN Ia dataset, the best fit values of the parameters p_s can be determined by a likelihood analysis, based on the calculation of

$$\begin{aligned} \chi^2(p_s, M') &\equiv \sum_{SN} \frac{\{\mu_{obs}(z_i) - \mu_{th}(p_s, z_i)\}^2}{\sigma_i^2} \\ &= \sum_{SN} \frac{\{5 \log_{10}[D_L(p_s, z_i)] - m_{obs}(z_i) + M'\}^2}{\sigma_i^2}, \end{aligned} \quad (\text{A7})$$

where $M' \equiv \mu_0 + M$ is a nuisance parameter which includes the absolute magnitude and the parameter h . The nuisance parameter M' can be marginalized over analytically [56] as

$$\bar{\chi}^2(p_s) = -2 \ln \int_{-\infty}^{+\infty} \exp \left[-\frac{1}{2} \chi^2(p_s, M') \right] dM',$$

resulting to

$$\bar{\chi}^2 = A - \frac{B^2}{C} + \ln \left(\frac{C}{2\pi} \right), \quad (\text{A8})$$

with

$$\begin{aligned} A &= \sum_{SN} \frac{\{5 \log_{10}[D_L(p_s, z_i)] - m_{obs}(z_i)\}^2}{\sigma_i^2}, \\ B &= \sum_{SN} \frac{5 \log_{10}[D_L(p_s, z_i)] - m_{obs}(z_i)}{\sigma_i^2}, \\ C &= \sum_{SN} \frac{1}{\sigma_i^2}. \end{aligned}$$

Relation (A7) has a minimum at the nuisance parameter value $M' = B/C$, which contains information of the values of h and M . Therefore, one can extract the values of h and M provided the knowledge of one of them. Finally, note that the expression

$$\chi_{SN}^2(p_s, B/C) = A - (B^2/C),$$

which coincides to (A8) up to a constant, is often used in the likelihood analysis [54, 56, 57], and thus in this case the results will not be affected by a flat M' distribution.

3. Baryon Acoustic Oscillation constraints

The Baryon Acoustic Oscillations are detected in the clustering of the combined 2dFGRS and SDSS main galaxy samples, and measure the distance-redshift relation at $z = 0.2$. Additionally, Baryon Acoustic Oscillations in the clustering of the SDSS luminous red galaxies measure the distance-redshift relation at $z = 0.35$. The observed scale of the BAO calculated from these samples, as well as from the combined sample, are jointly analyzed using estimates of the correlated errors to constrain the form of the distance measure $D_V(z)$ [29, 37, 58]

$$D_V(z) = c \left(\frac{z}{\Omega_k H(z)} \text{sinn}^2[\sqrt{|\Omega_k|} \int_0^z \frac{dz'}{H(z')}] \right)^{1/3}. \quad (\text{A9})$$

The peak positions of the BAO depend on the ratio of $D_V(z)$ to the sound horizon size at the drag epoch (where baryons were released from photons) z_d , which can be obtained by using a fitting formula [59]:

$$z_d = \frac{1291(\Omega_m h^2)^{0.251}}{1 + 0.659(\Omega_m h^2)^{0.828}} [1 + b_1(\Omega_b h^2)^{b_2}], \quad (\text{A10})$$

with

$$b_1 = 0.313(\Omega_m h^2)^{-0.419} [1 + 0.607(\Omega_m h^2)^{0.674}], \quad (\text{A11})$$

$$b_2 = 0.238(\Omega_m h^2)^{0.223}. \quad (\text{A12})$$

In this paper, we use the data of $r_s(z_d)/D_V(z)$, which are listed in Table III, where $r_s(z)$ is the comoving sound horizon size

$$\begin{aligned} r_s(z) &= c \int_0^t \frac{c_s dt}{a} = c \int_0^a \frac{c_s da}{a^2 H} = c \int_z^\infty dz \frac{c_s}{H(z)} \\ &= \frac{c}{\sqrt{3}} \int_0^{1/(1+z)} \frac{da}{a^2 H(a) \sqrt{1 + (3\Omega_b/(4\Omega_\gamma)a)}}, \end{aligned} \quad (\text{A13})$$

where c_s is the sound speed of the photon–baryon fluid [60–62]:

$$c_s^{-2} = 3 + \frac{9}{4} \times \frac{\rho_b(z)}{\rho_\gamma(z)} = 3 + \frac{9}{4} \times \left(\frac{\Omega_b}{\Omega_\gamma} \right) a, \quad (\text{A14})$$

and here $\Omega_\gamma = 2.469 \times 10^{-5} h^{-2}$ for $T_{CMB} = 2.725 K$.

z	$r_s(z_d)/D_V(z)$
0.2	0.1905 ± 0.0061
0.35	0.1097 ± 0.0036

TABLE III: The observational $r_s(z_d)/D_V(z)$ data [37].

Using the data of BAO in Table III and the inverse covariance matrix V^{-1} in [37]:

$$V^{-1} = \begin{pmatrix} 30124.1 & -17226.9 \\ -17226.9 & 86976.6 \end{pmatrix}, \quad (\text{A15})$$

Thus, the $\chi_{BAO}^2(p_s)$ is given as

$$\chi_{BAO}^2(p_s) = X^t V^{-1} X, \quad (\text{A16})$$

where X is a column vector formed from the values of theory minus the corresponding observational data, with

$$X = \begin{pmatrix} \frac{r_s(z_d)}{D_V(0.2)} - 0.1905 \\ \frac{r_s(z_d)}{D_V(0.35)} - 0.1097 \end{pmatrix}, \quad (\text{A17})$$

and X^t denotes its transpose.

4. Cosmic Microwave Background constraints

The CMB shift parameter R is provided by [63]

$$R(z_*) = \frac{\sqrt{\Omega_m H_0^2}}{\sqrt{|\Omega_k|}} \text{sinn}[\sqrt{|\Omega_k|} \int_0^{z_*} \frac{dz'}{H(z')}], \quad (\text{A18})$$

here, the redshift z_* (the decoupling epoch of photons) is obtained by using the fitting function [64]

$$z_* = 1048 [1 + 0.00124(\Omega_b h^2)^{-0.738}] [1 + g_1(\Omega_m h^2)^{g_2}],$$

where the functions g_1 and g_2 read

$$\begin{aligned} g_1 &= 0.0783(\Omega_b h^2)^{-0.238} (1 + 39.5(\Omega_b h^2)^{0.763})^{-1}, \\ g_2 &= 0.560 (1 + 21.1(\Omega_b h^2)^{1.81})^{-1}. \end{aligned}$$

In additional, the acoustic scale is related to the distance ratio and is expressed as

$$l_A = \frac{\pi}{r_s(z_*)} \frac{c}{\sqrt{|\Omega_k|}} \text{sinn}[\sqrt{|\Omega_k|} \int_0^{z_*} \frac{dz'}{H(z')}]. \quad (\text{A19})$$

	5 – year ML	5 – year mean	error, σ
$l_A(z_*)$	302.10	302.45	0.86
$R(z_*)$	1.710	1.721	0.019
z_*	1090.04	1091.13	0.93

TABLE IV: The observational l_A, R, z_* data [32].

Using the data of l_A, R, z_* in [32], which are listed in Table IV, and their covariance matrix of $[l_A(z_*), R(z_*), z_*]$ referring to [32]:

$$C^{-1} = \begin{pmatrix} 1.800 & 27.968 & -1.103 \\ 27.968 & 5667.577 & -92.263 \\ -1.103 & -92.263 & 2.923 \end{pmatrix}, \quad (\text{A20})$$

we can calculate the likelihood L as $\chi_{CMB}^2 = -2 \ln L$:

$$\chi_{CMB}^2 = \Delta d_i [C^{-1}(d_i, d_j)] [\Delta d_i]^t, \quad (\text{A21})$$

where $\Delta d_i = d_i - d_i^{data}$ is a row vector, and $d_i = (l_A, R, z_*)$.

5. OHD

The observational Hubble data are based on differential ages of the galaxies [65]. In [66], Jimenez *et al.* obtained an independent estimate for the Hubble parameter using the method developed in [65], and used it to constrain the EOS of dark energy. The Hubble parameter depending on the differential ages as a function of redshift z can be written in the form of

$$H(z) = -\frac{1}{1+z} \frac{dz}{dt}. \quad (\text{A22})$$

So, once dz/dt is known, $H(z)$ is obtained directly [67]. By using the differential ages of passively-evolving galaxies from the Gemini Deep Deep Survey (GDDS) [68] and archival data [69–74], Simon *et al.* obtained $H(z)$ in the range of $0.1 \lesssim z \lesssim 1.8$ [67]. In [41], Stern *et al.* used the new data of the differential ages of passively-evolving galaxies at $0.35 < z < 1$ from Keck observations, SPICES survey and VVDS survey. The twelve observational Hubble data from [40, 41, 67] are list in Table V. Here, we use the value of Hubble constant $H_0 = 74.2 \pm 3.6 \text{ km s}^{-1} \text{ Mpc}^{-1}$, which is obtained by observing 240 long-period Cepheids in [40]. As pointed out in [40], the systematic uncertainties have been greatly reduced by the unprecedented homogeneity in the periods and metallicity of these Cepheids. For all Cepheids, the same instrument and filters are used to reduce the systematic uncertainty related to flux calibration. In addition,

z	0	0.1	0.17	0.27	0.4	0.48	0.88	0.9	1.30	1.43	1.53	1.75
$H(z)$ (km s ⁻¹ Mpc ⁻¹)	74.2	69	83	77	95	97	90	117	168	177	140	202
1σ uncertainty	± 3.6	± 12	± 8	± 14	± 17	± 60	± 40	± 23	± 17	± 18	± 14	± 40

TABLE V: The observational $H(z)$ data [40, 41].

in [39], the authors took the BAO scale as a standard ruler in the radial direction, called "Peak Method", obtaining three more additional data: $H(z = 0.24) = 79.69 \pm 2.32$, $H(z = 0.34) = 83.8 \pm 2.96$, and $H(z = 0.43) = 86.45 \pm 3.27$, which are model and scale independent. Here, we just consider the statistical errors.

The best fit values of the model parameters from observational Hubble data [67] are determined by minimizing

$$\chi_{Hub}^2(p_s) = \sum_{i=1}^{15} \frac{[H_{th}(p_s; z_i) - H_{obs}(z_i)]^2}{\sigma^2(z_i)}, \quad (\text{A23})$$

where p_s denotes the parameters contained in the model, H_{th} is the predicted value for the Hubble parameter, H_{obs} is the observed value, $\sigma(z_i)$ is the standard deviation measurement uncertainty, and the summation is over the 15 observational Hubble data points at redshifts z_i .

-
- [1] A. G. Riess *et al.*, *Astron. J.* **116** 1009 (1998) [astro-ph/9805201].
 - [2] S. Perlmutter *et al.*, *Astrophys. J.* **517** 565 (1999) [astro-ph/9812133].
 - [3] D. N. Spergel *et al.*, *Astrophys. J. Supp.* **148** 175 (2003) [astro-ph/0302209].
 - [4] D. N. Spergel *et al.*, *Astrophys. J. Supp.* **170** 377 (2007) [astro-ph/0603449].
 - [5] M. Tegmark *et al.*, *Phys. Rev. D* **69** 103501 (2004) [astro-ph/0310723].
 - [6] M. Tegmark *et al.*, *Astrophys. J.* **606** 702 (2004) [astro-ph/0310725].
 - [7] H. K. Jassal, J. S. Bagla and T. Padmanabhan, [astro-ph/0601389].
 - [8] T. M. Davis *et al.*, *Astrophys. J.* **666** 716 (2007) [astro-ph/0701510].
 - [9] L. Samushia and B. Ratra, arXiv:0803.3775 [astro-ph.CO].
 - [10] P. J. E. Peebles and B. Ratra, *Astrophys. J. Lett.* **325** L17 (1988).
 - [11] B. Ratra and P. J. E. Peebles, *Phys. Rev. D* **37** 3406 (1988).
 - [12] I. Zlatev, L. Wang and P. J. Steinhardt, *Phys. Rev. Lett.* **82** 896 (1999) [astro-ph/9807002].
 - [13] P. J. Steinhardt, L. Wang and I. Zlatev, *Phys. Rev. D* **59** 123504 (1999) [astro-ph/9812313].
 - [14] M. S. Turner, *Int. J. Mod. Phys. A* **17S1** 180 (2002) [astro-ph/0202008].
 - [15] V. Sahni, *Class. Quant. Grav.* **19** 3435 (2002) [astro-ph/0202076].
 - [16] R. R. Caldwell, M. Kamionkowski and N. N. Weinberg, *Phys. Rev. Lett.* **91** 071301 (2003) [astro-ph/0302506].
 - [17] B. Feng *et al.*, *Phys. Lett. B* **607** 35 (2005) [astro-ph/0404224].
 - [18] S. D. H. Hsu, *Phys. Lett. B* **594** 13 (2004) [hep-th/0403052].
 - [19] M. Li, *Phys. Lett. B* **603** 1 (2004) [hep-th/0403127].

- [20] R. G. Cai, *Phys. Lett. B* **657** 228 (2007).
- [21] H. Wei and R. G. Cai, *Phys. Lett. B* **660** 113 (2008).
- [22] C. Gao, X. Chen and Y. G. Shen, *Phys. Rev. D* **79** 043511 (2009).
- [23] L. Xu, W. Li, J. Lu and B. Chang, *Mod. Phys. Lett. A* **24** 1355 (2009).
- [24] W. M. Wood-Vasey *et al.*, *Astrophys. J.* **666** 694 (2007) [astro-ph/0701041].
- [25] A. G. Riess *et al.* [Supernova Search Team Collaboration], *Astrophys. J.* **607** 665 (2004) [astro-ph/0402512].
- [26] P. Astier *et al.*, *Astron. Astrophys.* **447** 31 (2006) [astro-ph/0510447].
- [27] A. G. Riess *et al.*, *Astrophys. J.* **659** 98 (2007) [astro-ph/0611572].
- [28] Y. Wang and P. Mukherjee, *Astrophys. J.* **650** 1 (2006) [astro-ph/0604051].
- [29] D. J. Eisenstein *et al.*, [SDSS Collaboration], *Astrophys. J.* **633** 560 (2005) [astro-ph/0501171].
- [30] X. Zhang, *Phys. Rev. D* **79** 103509 (2009).
- [31] M. Suwa and T. Nihe, arXiv:0911.4810 [astro-ph.CO].
- [32] E. Komatsu *et al.*, [WMAP Collaboration], *Astrophys. J. Suppl.* **180** 330 (2009).
- [33] L. Xu, J. Lu and W. Li, *Eur. Phys. J. C* **64** 89 (2009).
- [34] W. J. Percival *et al.*, *Mon. Not. R. Astron. Soc.* **381** 1053 (2007) arXiv:0705.3323 [astro-ph.CO].
- [35] M. Li, X. Li and X. Zhang, arXiv:0912.3988 [astro-ph.CO].
- [36] M. Hicken *et al.*, *Astrophys. J.* **700** 1097 (2009).
- [37] W. J. Percival *et al.*, arXiv:0907.1660 [astro-ph.CO].
- [38] S. W. Allen, D. A. Rapetti, R. W. Schmidt, H. Ebeling, R. G. Morris and A. C. Fabian, *Mon. Not. Roy. Astron. Soc.* **383** 879 (2008).
- [39] E. Gaztanaga *et al.*, arXiv:0807.3551 [astro-ph.CO].
- [40] A. G. Riess *et al.*, arXiv:0905.0695 [astro-ph.CO].
- [41] D. Stern *et al.*, arXiv:0907.3149 [astro-ph.CO].
- [42] A. Lewis and S. Bridle, *Phys. Rev. D* **66** 103511 (2002); URL: <http://cosmologist.info/cosmomc/>.
- [43] D. Rapetti, S. W. Allen and J. Weller, *Mon. Not. Roy. Astron. Soc.* **360** 555 (2005).
- [44] URL: http://www.stanford.edu/~drapetti/fgas_module/
- [45] S. Burles, K. M. Nollett and M. S. Turner, *Astrophys. J.* **552** L1 (2001).
- [46] M. Biesiada 2007 *J. Cos. Astro. Phys.* **0702** 003.
- [47] A. R. Liddle *Mon. Not. Roy. Astron. Soc.* **351** L49 2004.
- [48] W. Godlowski, M. Szydlowski 2005 *it Phys. Lett. B* **623** 10; M. Szydlowski, W. Godlowski 2006 *Phys. Lett. B* **633** 427.
- [49] M. Szydlowski, A. Kurek and A. Krawiec 2006 *Phys. Lett. B* **642** 171; M. Szydlowski, A. Kurek astro-ph/0603538.
- [50] L. X. Xu, C. W. Zhang and H. Y. Liu, *Chin. Phys. Lett.* **24** 2459 (2007).
- [51] S. Nesseris and L. Perivolaropoulos, *JCAP* **0701** 018 (2007) [astro-ph/0610092].
- [52] M. Kowalski *et al.*, *ApJ*, **686** 749 (2008).
- [53] J. Guy, P. Astier, S. Nobili, N. Regnault and R. Pain, *A&A* **443** 781 (2005).
- [54] E. Garcia-Berro, E. Gaztanaga, J. Isern, O. Benvenuto and L. Althaus, astro-ph/9907440; A. Riazuelo and J. Uzan, *Phys. Rev. D* **66** 023525 (2002); V. Acquaviva and L. Verde, *JCAP* **0712** 001 (2007).
- [55] R. Gannouji and D. Polarski, *JCAP* **0805** 018 (2008).
- [56] S. Nesseris and L. Perivolaropoulos, *Phys. Rev. D* **72** 123519 (2005); L. Perivolaropoulos, *Phys. Rev. D* **71** 063503 (2005); E. Di Pietro and J. F. Claeskens, *Mon. Not. Roy. Astron. Soc.* **341** 1299 (2003); A. C. C. Guimaraes, J. V. Cunha and J. A. S. Lima, *JCAP* **0910** 010 (2009).
- [57] L. Xu, W. Li and J. Lu, *JCAP* **0907** 031 (2009).
- [58] T. Okumura, T. Matsubara, D. J. Eisenstein, I. Kayo, C. Hikage, A. S. Szalay and D. P. Schneider, *Astrophys. J.* **676** 889 (2008).
- [59] D. J. Eisenstein and W. Hu, *Astrophys. J.* **496** 605 (1998).
- [60] W. Hu and N. Sugiyama, *Astrophys. J.* **444** 489 (1995) [arXiv:astro-ph/9407093].
- [61] W. Hu, M. Fukugita, M. Zaldarriaga and M. Tegmark, *Astrophys. J.* **549** 669 (2001) [arXiv:astro-ph/0006436].
- [62] R. R. Caldwell and M. Doran, *Phys. Rev. D* **69** 103517 (2004).
- [63] J. R. Bond, G. Efstathiou and M. Tegmark, *Mon. Not. Roy. Astron. Soc.* **291** L33 (1997).
- [64] W. Hu and N. Sugiyama, *Astrophys. J.* **471** 542 (1996).
- [65] R. Jimenez and A. Loeb, *Astrophys. J.* **573** 37 (2002) [astro-ph/0106145].
- [66] R. Jimenez, L. Verde, T. Treu and D. Stern, *Astrophys. J.* **593** 622 (2003) [astro-ph/0302560].
- [67] J. Simon, L. Verde and R. Jimenez, *Phys. Rev. D* **71** 123001 (2005) [astro-ph/0412269].
- [68] R. G. Abraham *et al.*, *Astron. J.* **127** 2455 (2004) [astro-ph/0402436].
- [69] T. Treu, M. Stiavelli, S. Casertano, P. Moller and G. Bertin, *Mon. Not. Roy. Astron. Soc.* **308** 1037 (1999).
- [70] T. Treu, M. Stiavelli, P. Moller, S. Casertano and G. Bertin, *Mon. Not. Roy. Astron. Soc.* **326** 221 (2001) [astro-ph/0104177].
- [71] T. Treu, M. Stiavelli, S. Casertano, P. Moller and G. Bertin, *Astrophys. J. Lett.* **564** L13 (2002).
- [72] J. Dunlop, J. Peacock, H. Spinrad, A. Dey, R. Jimenez, D. Stern and R. Windhorst, *Nature* **381** 581 (1996).
- [73] H. Spinrad, A. Dey, D. Stern, J. Dunlop, J. Peacock, R. Jimenez and R. Windhorst, *Astrophys. J.* **484** 581 (1997).
- [74] L. A. Nolan, J. S. Dunlop, R. Jimenez and A. F. Heavens, *Mon. Not. Roy. Astron. Soc.* **341** 464 (2003) [astro-ph/0103450].